Unified database of radiative recombination and photoionization data for low-charged tungsten ions in plasmas. Atoms in laser and fusion plasmas

M. B. Trzhaskovskaya
Department of Theoretical Physics
Petersburg Nuclear Physics Institute, Gatchina 188300, Russia

V. K. Nikulin
Division of Plasma Physics, Atomic Physics, and Astrophysics
A.F.Ioffe Physical-Technical Institute, St.Petersburg 194021, Russia

Research Coordination Meeting on CRP
"Spectroscopic and Collisional Data for Tungsten in Plasma from 1 eV to 20 keV"

IAEA, Vienna, Austria, 6–8 October, 2014

Introduction

In a time of the CRP execution, we performed the following studies.

1. The unified database of the radiative recombination and photoionization cross sections, radiative recombination rates, and radiated power loss rates for impurity ions was supplemented with the data for 62 tungsten ions in the range W^{6+} – W^{74+}.

2. We estimated the impact of the core electrons polarization involved in radiative recombination on RRCS (PRR effect). It was shown that the inclusion of the PRR channel in RRCS calculations for Fe XVII eliminates the discrepancy between experimental and theoretical values of the electron-impact excitation cross section. The PRR effect was assessed for highly-charged tungsten ions in the non-resonance energy ranges. The enhancement RRCS due to the PRR effect depends on the photon energy, the principal quantum number of polarized shells, and the ion charge.

3. We studied the influence of plasmas temperature and densiy on the energy spectrum and level occupation numbers of an ion in Local Termodynamic Equilibrium (LTE) plasmas. Comparison was performed for the mean ionization stages of the Fe ions obtained by various codes in the LTE regimes. New calculations were carried out for the impurity tungsten ion in fusion plasma at low temperature as well as for the dense tungsten plasma in the wide temperature range.

[1] M.B. Trzhaskovskaya, V.K. Nikulin, R.E.H. Clark, Chapter *"Accurate Data on Radiative Recombination and Photoionization for Highly-Charged Tungsten Ions in Plasmas"* in book *"Horizons in World Physics"*, Ed.A.Reimer, vol.277 (Nova, N.-Y., 2012).

[2] V.K.Nikulin, M.B.Trzhaskovskaya, "*Comment on "Energy Dependent Excitation Cross Section Measurements of Diagnostic Lines of Fe XVII"*. Phys.Rev.Lett. **108** (2012) 139301.

[3] M.B. Trzhaskovskaya and V.K. Nikulin, "*Polarization Radiative Recombination Effect for Tungsten Highly-Charged Ions*", PNPI Report No PNPI-2893, 23p. (2012).

[4] M.B. Trzhaskovskaya and V.K. Nikulin, "*Radiative Recombination Data for Tungsten ions: I. W^{24+}–W^{45+}*". At. Data Nucl. Data Tables 99 (2013) 249.

[5] M.B. Trzhaskovskaya and V.K. Nikulin, "*Atom in dense laser and fusion plasmas*", PNPI Report No PNPI-2932, 26p. (2013).

[6] M.B. Trzhaskovskaya and V.K. Nikulin, "*Radiative Recombination Data for Tungsten ions: II. W^{47+}–W^{71+}*". At. Data Nucl. Data Tables 100 (2014) 986.

[7] M.B. Trzhaskovskaya and V.K. Nikulin, "*Radiative Recombination Data for Tungsten ions: III. W^{14+}–W^{23+}*". At. Data Nucl. Data Tables (2014) (in press).

[8-16] M.B. Trzhaskovskaya, V.K. Nikulin, Nine Petersburg Nuclear Physics Institute Reports: "*Radiative Recombination and Photoionization Data for Tungsten Ions, parts I-IX*", Nos 2876,2863,2866,2867,2869 (2011); Nos 2894,2895 (2012); Nos 2947,2948 (2014).

Radiative recombination and photoionization data

The database for the RR and photoionization data includes total RR cross sections (RRCS), fit parameters for partial photoionization cross sections (PCS), as well as partial and total RR rate coefficients (RR rates) and radiated power loss rate coefficients (RPL rates). Total RRCS are calculated in the electron energy range from 1 eV to ∼80 keV. RR and RPL rates are presented in the temperature range from 10^4 K to 10^9 K.

Currently we were concerned with the comparatively low-charged tungsten ions from W^{6+} to W^{23+}. A peculiarity of the ions is that RRCS, PCS, as well as RR/RPL rates may be non-monotonic functions of an electron energy. Such ions are more difficult for calculation and especially difficult for fitting.

As earlier, calculations are based on the fully relativistic treatment of photoionization and RR. All significant multipoles of the radiative field are taken into account. We use the average-configuration Dirac-Fock (DF) method with the exact consideration of the electron exchange for calculations of the bound and continuum electron wave functions. Values of RR rates and RPL rates are found using the thermal average over relativistic PCS provided the continuum electron velocity is described by the relativistic Maxwell-Jüttner distribution.

The exact consideration of the electron exchange has been shown to be of importance in the RR and photoionization calculations for low-charged ions especially at low energies. For example, in the case of W^{6+}, partial RR and photoionization cross sections, obtained taking into account the exact and approximate exchange may differ by several times at electron energies $E_k \lesssim 200$ eV and up by $\sim 70\%$ at high electron energy ~ 20 keV.

On the contrary, relativistic and multipole effects are of importance for highly-charged ions and at high energies. In particular, the relativistic Maxwell-Jüttner distribution used for the first time by us in the RR/RPL rate calculations, decreases the rates considerably at a high temperature as compared with the commonly used non-relativistic Maxwell-Boltzmann distribution, the decreasing being $\sim 25\%$ at the temperature $T = 10^9$ K.

Our calculations were performed for the most stable tungsten ions. For each an ion W^{q+}, the electron configuration with the lowest theoretical total energy was found using the Dirac-Fock method with regard to the Breit magnetic interaction between electrons. For all ions, configurations are in line with the corresponding ones presented in compilation [Kramida and Shirai (2009)].

To have a chance of getting partial cross sections at an any energy, PCS for all electron states with principal quantum numbers $n \le 10$ and orbital momenta $\ell \le 4$ were fitted by an analytical expression with five fit parameters. Partial RRCS may be also found by the use of the fit parameters and the relationship between RRCS $\sigma_{\rm rr}^{(n\ell j)}$ for a recombining ion W^{q+} and PCS $\sigma_{\rm ph}^{(n\ell j)}$ for the associated recombined ion $W^{(q-1)+}$ which makes up as the recombining ion with one additional electron in the shell with quantum numbers n, ℓ, and j:

$$W^{(q-1)+} = W^{q+} + (n\ell j)\,. \tag{1}$$

We use the relativistic relationship between PCS and RRCS which has the following form

$$\sigma_{\rm rr}^{(n\ell j)} = \frac{k^2}{2m_0c^2E_{\rm k} + E_{\rm k}^2}\,{\rm v}^{(n\ell j)}\sigma_{\rm ph}^{(n\ell j)}\,, \tag{2}$$

where k is the photon energy, E_k is the kinetic electron energy, and ${\rm v}^{(n\ell j)}$ is the number of vacancies in the $n\ell j$ shell prior to recombination.

The analytical expression for fitting PCS in the $n\ell j$ shell may be written as:

$$\sigma_{\rm ph}^{(n\ell j)}(k) = \sigma_0\Big\{\Big[(k/k_0-1)^2 + y_w^2\Big]\Big(k/k_0\Big)^{0.5p-\ell-5.5}\Big[1+\sqrt{k/(k_0y_{\rm a})}\Big]^{-p}\Big\}\,, \tag{3}$$

where σ_0, k_0, $y_{\rm w}$, p, and $y_{\rm a}$ are fit parameters. With Eq. (3), the fit parameters were found by minimizing the mean-square deviation of fitted PCS from calculated values with the simplex search method.

The fitting has been performed in the following range of the photon energy

$$E_{\rm th} + 1\,{\rm eV} \le k \le k_{\rm max}\,, \tag{4}$$

where $E_{\rm th}$ is the ionization threshold energy. The value $k_{\rm max}$ is determined by decreasing PCS $\sigma_{\rm ph}^{(n\ell j)}(k_{\rm max})$ as compared with its maximum by five/six orders of magnitude. Usually, $k_{\rm max}$ is $\sim 100E_{\rm th}$ for the s, p, and d states and $\sim 40E_{\rm th}$ for the f and g states. Consequently, the fit parameters and Eq. (3) allow one to obtain PCS as well as RRCS for any value of $k \le k_{\rm max}$.

The real root-mean-square (rms) error of the fitting $\delta_{\rm av}$ was found for each a state. As a rule, $\delta_{\rm av} \lesssim 2\%$. However for low-charged ions, for example W^{6+}, the error may be larger reaching 10%.

Total RRCS $\sigma_{\rm tot}(E_{\rm k})$ as well as total RR rates $\alpha_{\rm tot}(kT)$ and RPL rates $\gamma_{\rm tot}(kT)$ are determined by summation of partial values over all electron states beginning from the lowest open shell up to shells with the principal quantum number $n = 20$ as follows:

$$\sigma_{\rm tot}(E_{\rm k}) = \sum_{n=n_{\rm min}}^{20}\sum_{\kappa=\mp1,\mp2,\ldots,-n}\sigma_{\rm rr}^{(n\ell j\equiv n\kappa)}(E_{\rm k})\,, \tag{5}$$

where $\kappa = (\ell - j)(2j+1)$ is the relativistic quantum number and $n_{\rm min}$ along with a corresponding value of κ refer to the ground state.

It is convenient to use in fusion studies an analytical expression for total RR rates. So total RR rates for all tungsten ions were fitted by the following expression:

$$\alpha_{\rm tot}(T) = a\Big[\sqrt{T/T_0}\,(1+\sqrt{T/T_0})^{1.5-b}(1+\sqrt{T/T_1})^{2.5+b}\Big]^{-1}\,, \tag{6}$$

the fit parameters a, b, T_0, and T_1 along with the rms error were calculated.

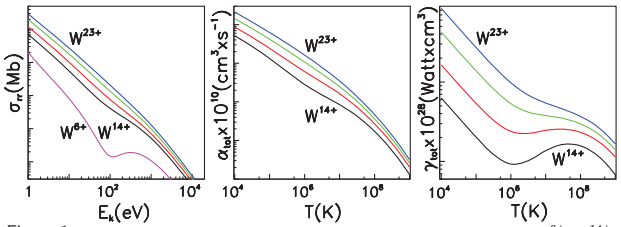

Figure 1: Total RRCS, RR rates, and RPL rates for representative tungsten ions W^{6+}, W^{14+}, W^{17+}, W^{20+}, and W^{23+}.

Fig. 1 present RRCS, RR rates, and RPL rates for five/four comparatively low-charged tungsten ions in the charge range $6 \le q \le 23$. As is seen, curves $\sigma_{\rm tot}(E_{\rm k})$ and $\alpha_{\rm tot}(kT)$ for ions with $q \lesssim 20$ have noticeable bends in the range ∼100-300 eV. This tendency brings into existence minima and maxima in the $E_{\rm k}$-dependence of $\sigma_{\rm tot}$ and in the kT-dependence of $\alpha_{\rm tot}$ for the W^{6+} ion. As is evident, the behavior of total RPL rates is non-monotonic even for ions W^{14+} - W^{17+}. This structure is caused by behavior of the associated partial cross sections and rates. Displayed in **Fig. 2** are

partial RRCS for states contributing significantly to total RRCS for W^{6+} and W^{14+}.

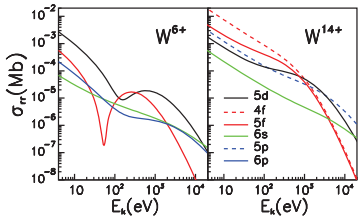

Figure 2: Partial RRCS for the low electron states of W^{6+} and W^{14+}.

One can see that non-monotony in $\sigma_{rr}^{n\ell j}$ for W^{6+} and the bent $E_{\rm k}$-dependence for the $5p_{3/2}$, $5d_{5/2}$, and $5f_{7/2}$ shells at $E_{\rm k} \gtrsim 100$ eV for W^{14+} manifests itself in total RRCS. It is these irregularities that are typical for low-charged ions. It should be also noted that an increase of the rms fitting error $\delta_{\rm av}$ is just due to such behavior of partial and total magnitudes.

Temperature influence on the energy spectrum and level occupations of an ion in plasmas

Our goal was to study the influence of a plasmas temperature and density on the energy spectrum and level occupation numbers of the tungsten ions in LTE plasmas. With this in mind, the code PLASMASATOM have been designed on the basis of our suite of computer codes RAINE (Relativistic Atom. Interaction of electromagnetic radiation and Nucleus with atomic Electrons). The code PLASMASATOM is based on the average-atom model. The model has been employed in the Los Alamos INFERNO code [D.A. Liberman (1982); B.I. Bennet and D.A. Liberman (1985)], PURGATORIO code [B. Wilson *et al.* (2006)], and more advanced PARADISIO code [M. Pénicaud (2009)].

In the average-atom model, the plasma is taken to consist of the neutral WS cells. Each of them contains a nucleus with a charge Z and Z electrons, some of them being in bound states and some in continuum states. The continuum density is finite at the WS cell boundary and merges into the uniform free-electron density outside the cell. So we treat an isolated neutral cell in a local thermodynamic average sense neglecting the interaction of the cell with other ones. The radius of the WS cell $R_{\rm WS}$ is determined from the material density and atomic weight.

Methods of calculations

In the relativistic Dirac-Slater theory, each an electron is assumed to satisfy the central-field system of the Dirac equations which may be written as

$$\begin{aligned} \frac{dG(r)}{dr} &= -\frac{\kappa}{r}G(r) + [E + 1 - V(r)]F(r)\,, \\ \frac{dF(r)}{dr} &= \frac{\kappa}{r}F(r) - [E - 1 - V(r)]G(r)\,. \end{aligned} \qquad (7)$$

Here $G(r)$ and $F(r)$ are the large and small components of the electron wave function multiplied by r, E is the total electron energy including the rest mass, and $V(r)$ is the potential electron energy. We used relativistic units, $\hbar = c = m_0 = 1$. The potential with the exchange term in the local density approximation is written as

$$V(r) = \begin{cases} -\frac{\alpha Z}{r} + \frac{\alpha}{r}\left[\int_0^r 4\pi r^2\rho(r)dr + r\int_r^{R_{\rm WS}} 4\pi r\rho(r)dr\right] - \alpha\left[\frac{3}{\pi}\rho(r)\right]^{1/3}, & r \le R_{\rm WS}, \\ 0, & r > R_{\rm WS}\,. \end{cases} \qquad (8)$$

Inside the WS cell, $\rho(r)$ is the total electron density, that is

$$\rho(r) = \rho_b(r) + \rho_c(r)\,. \qquad (9)$$

The bound density contribution may be written as

$$4\pi r^2\rho_b(r) = \sum_i (2j_i + 1) f_i(\varepsilon_i, \mu)[G_i^2(r) + F_i^2(r)]\,, \qquad (10)$$

where index i refers to the i-th electron state, and the Fermi–Dirac factor $f_i(\varepsilon_i, \mu)$ is given by the Fermi distribution:

$$f_i(\varepsilon_i, \mu) = \left[1 + \exp\left(\frac{\varepsilon_i - \mu}{kT}\right)\right]^{-1}. \qquad (11)$$

Here $\varepsilon_i < 0$ is the electron binding energy, μ is the chemical potential, kT is the temperature, and k is the Boltzmann constant. The occupation number of the i-th level is determined by

$$N_i = (2j_i + 1) f_i(\varepsilon_i, \mu). \qquad (12)$$

Bound electron wave functions are normalized so that

$$\int_0^{R_{\rm WS}} [G_i^2(r) + F_i^2(r)]dr = 1\,. \qquad (13)$$

The continuum density contribution evaluated by the DS method has the form

$$4\pi r^2\rho_c(r) = \int_0^\infty d\varepsilon f(\varepsilon, \mu) \sum_{\kappa=\pm1}^{\infty} 2|\kappa|[G_\kappa^2(r) + F_\kappa^2(r)]\,. \qquad (14)$$

Here $\varepsilon = E - 1 > 0$ and the relevant Fermi-Dirac factor $f(\varepsilon, \mu)$ takes the form:

$$f(\varepsilon, \mu) = \left[1 + \exp\left(\frac{\varepsilon - \mu}{kT}\right)\right]^{-1}. \qquad (15)$$

To eliminate the need of a direct calculations of the sum which converges slowly, we transformed Eq. (14) according to [T. Blensky and K. Ishikawa (1995)]. As a result of the rearrangement, the continuum density ρ_c may be written as

$$\rho_c(r) \approx \int_0^\infty d\varepsilon f(\varepsilon, \mu) \times \left\{ \sum_{\kappa=\pm1}^{\kappa_{\max}} \frac{|\kappa|}{2\pi}\left[\frac{G_\kappa^2 + F_\kappa^2}{r^2} - \frac{(E+1)p}{\pi}\left(j_\ell^2(pr) + \frac{E-1}{E+1}j_{\bar\ell}^2(pr)\right)\right] + \frac{Ep}{\pi^2}\right\}, \qquad (16)$$

where $j_\ell(pr)$ is the spherical Bessel function, $\bar\ell = 2j - \ell$, and $p = \sqrt{E^2 - 1}$. We checked that adoption of Eq. (16) permits to restrict to $\kappa_{\max} = 15$ to reach the prescribed accuracy rather than several tens or even hundreds of κ-terms required for the direct summation.

The chemical potential μ involving in the Fermi-Dirac factors (11) and (15) is determined provided that the cell with the radius $R_{\rm WS}$ has to be electrically neutral to give

$$F(\mu) = Z - 4\pi\int_0^{R_{\rm WS}} r^2\rho(r)dr = 0\,. \qquad (17)$$

Calculations based on Eqs.(7)–(17) will be denoted below by the DS–DS method.

Because of the computational burden of the DS continuum density calculations, we

have also elaborated the second version of code PLASMASATOM where ρ_c is evaluated within the framework of the semi-classical Thomas–Fermi (TF) approximation according to paper [W.R. Johnson (2001)]. Such calculations will be denoted by the DS–TF method.

In both methods, relevant equations are solved by the SCF method to obtain the electron potential $V(r)$, the chemical potential μ, and the total electron density $\rho(r)$. As usually, the iterative method is used.

Results and Discussion

We verified our results by comparing with calculations by Johnson [W.R. Johnson (2001,2006)] for iron and aluminium. The bound, continuum, and total densities for the iron ion in plasmas with the normal density at $kT = 100$ eV are shown in Fig. 3.

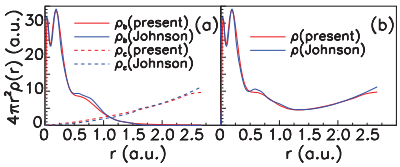

Figure 3: The bound and continuum electron densities (a) and the total density (b) calculated using the DS–TF method for the iron ion in laser plasmas at temperature $kT = 100$ eV and the normal density (0.85×10^{23} cm^{-3}).

We see that all our results (red curves) are very close to relevant results by Johnson (blue curves). The slight differences occur in ρ_b in ranges of maxima and minima where electron wave functions are usually very sensitive to all details of calculations and in ρ_c near the very boundary of the WS cell.

Besides, data in the Table allow one to compare the results obtained by the DS–DS and DS–TF methods. As is seen, in this case, there is a minor difference between the DS–DS and DS–TF results. The largest difference ($\sim 5\%$) occurs for the binding energy of the valence $4s$ shell. Values of μ obtained in the two methods differ by $\lesssim 0.3\%$ and values of the charge q only by $\sim 0.2\%$. It should be noted that all levels and the chemical potential become lower as well as the charge increases when passing from the DS–TF method to the DS–DS one.

As is known, the two continuum densities diverge drastically, $\rho_c(r)$ obtained by the DS method being oscillating function of r while ρ_c calculated by the TF method being a quite smooth function. However in spite of this fact, the results obtained using the DS–TF and DS–DS methods are very close to each other.

In addition, we compare our ion charge q for iron in three cases listed in Table 2 with mean ionization stages $< q >$ obtained by eight groups from Los Alamos, Livermore and Opacity Project (OPAC collaboration). The results were calculated with different eleven codes to prepare LULI[1] 2010 experiments (see [D.Gilles *et al.* (2011)]) and are useful for astrophysics.

[1] Laboratoire pour L'Utilization des Lasers Intenses

Our values (code 12 and asterisks) correlate with previous calculations. The difference in the mean ionization stage obviously imply the discrepancy between the frequency-dependent opacity. Besides, the data of Table 2 show that our results are in excellent agreement with the OP values of $< q >$. The largest difference is 4%.

In Fig. 5, we compare $N_{\rm bound}(kT) = \sum_i N_i = Z - q$ for the uranium atom with results obtained by [M. Pénicaud (2009)] using code PARADISIO at the low density $\rho = 0.01$g/cm^3 ($2.5\cdot10^{19}$ cm^{-3}). Our calculation is in excellent agreement with the previous results in the range 0.1 eV – 10 keV. In Fig. 5(b), new results for the tungsten ion at the same density ($3.3\cdot10^{19}$cm^{-3}) are presented. Here it should be noted a considerable decreasing $N_{\rm bound}$ in the temperature range 10 eV – 2 keV.

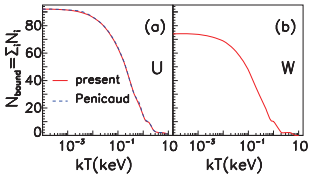

Figure 5: A number of bound electrons, that is $Z - q$, for ions of uranium (a) and of tungsten (b).

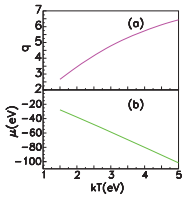

Figure 6: The charge q (a) and the chemical potential μ (b) for the impurity tungsten ion.

In Fig. 6, the ion charge q (a) and the chemical potential μ (b) are displayed in the temperature range $kT = 1.5 - 5.0$ eV. As is evident, values of the charge and chemical potential change noticeably when the temperature increases.

Table 1. Spectrum of binding energies ε_i, level populations N_i, $N_{\rm bound} = \Sigma_i N_i$, the charge q, and the chemical potential μ for the iron ion at $kT = 100$ eV and $R_{\rm WS} = 2.67$ a.u.

	Present				Johnson (2001)	
	DS–DS		DS–TF		DS–TF	
Shell	ε_i(a.u.)	N_i	ε_i(a.u.)	N_i	ε_i(a.u.)	N_i
$1s$	-261.305	2.0000	-261.289	2.0000	-261.251	2.0000
$2s$	-34.247	1.9986	-34.232	1.9986	-34.205	1.9988
$2p_{1/2}$	-30.239	1.9957	-30.214	1.9957	-30.186	1.9964
$2p_{3/2}$	-29.764	3.9903	-29.749	3.9903	-29.721	3.9919
$3s$	-6.248	0.8122	-6.239	0 8147	-6.246	0.9087
$3p_{1/2}$	-5.008	0.6559	-4.999	0 6581	-5.005	0.7453
$3p_{3/2}$	-4.929	1.2928	-4.920	1.2973	-4.926	1.4707
$3d_{3/2}$	-2.954	0.8725	-2.943	0.8757	-2.945	1.0131
$3d_{5/2}$	-2.942	1.3054	-2.931	1.3103	-2.933	1.5159
$4s$	-0.627	0.2580	-0.593	0.2577	-0.351	0.2868
$N_{\rm bound}$		15.1814		15.1985		15.9277
q		10.8186		10.8015		10.0723
μ (a.u.)	–7.6452		–7.6169		–6.9187	

As is seen, our results obtained using the DS–TF method correlate well with data by Johnson. The largest difference is for the binding energy of the valence $4s$ level.

Table 2. Comparison of mean ionization stages $<q>$ for Fe obtained by us with those from OP [M.J.Seaton, R.M.Badnell (2004)]. N_e=3.16·10^{20}cm^{-3}.

Case	kT,eV	ρ, mg/cm^3	$< q >$, present	$< q >$, OP
1	15.3	5.48	5.58	5.35
2	27.3	3.39	8.69	8.65
3	38.5	2.63	11.22	11.2

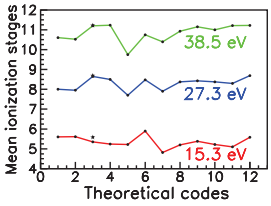

Figure 4: Iron mean ionization stages $< q >$ obtained by eleven codes. Codes used are: 1:FLYCHK (NLTE), 2:FLYCHK (LTE), 3:OP + our results ($\star$), 4:STA, 5:AA-Z_P, 6:AA-Z_M, 7:CASSANDRA, 8:OPAS, 9:SCO(rel.), 10:SCO-RCG, 11:LEDCOP, 12:Present calculations,PLASMASATOM. Codes 5,6 and 12 are LTE Average Atom ionization models. Figure is taken from [D.Gilles *et al.* (2011)].

Tungsten impurities in fusion plasmas

To study tungsten impurities in fusion plasmas, we use the non-linear SCF screening model [M.W.C. Dharma-Wardana (1991)], [F. Perrot (1982)] for calculation of the screening impurity potential. In the model, impurities in plasmas are considered as neutral pseudo-atoms. $R_{\rm WS}$ is assumed to be large. The chemical potential μ is found before the SCF calculations on the basis of the prescribed plasmas density N_e and temperature kT using the following expression [F. Perrot (1982)]

$$N_e = \frac{\sqrt{2}}{\pi^2}(kT)^{3/2}\int_0^\infty \frac{y^{1/2}dy}{1+\exp(y-\mu/kT)}, \qquad (18)$$

We consider the typical tokamak plasmas density $N_e = 10^{14}$cm^{-3} and the temperature range 1 eV$\leq kT \leq$ 5 eV. The SCF potential $V(r)$ and the total electron density $\rho(r)$ are found by the iterative process described above. The DS–DS method is used.

Table 3. Spectrum of energies ε_i and level populations N_i for the tungsten ion at low temperatures (kT =2, 3 eV) as well as for a free neutral tungsten atom ($kT = 0$).

kT(eV)	0.0		2.0		3.0	
Shell	ε_i(eV)	N_i	ε_i(eV)	N_i	ε_i(eV)	N_i
$4s$	-566.71	2.0	-601.09	2.0000	-621.06	2.0000
$4p_{1/2}$	-470.77	2.0	-505.15	2.0000	-525.13	2.0000
$4p_{3/2}$	-402.85	4.0	-437.23	4.0000	-457.21	4.0000
$4d_{3/2}$	-244.71	4.0	-279.10	4.0000	-299.07	4.0000
$4d_{5/2}$	-232.20	6.0	-266.58	6.0000	-286.56	6.0000
$4f_{5/2}$	-34.17	6.0	-68.50	6.0000	-88.39	6.0000
$4f_{7/2}$	-31.93	8.0	-66.26	8.0000	-86.13	7.9992
$5s$	-78.80	2.0	-112.82	2.0000	-132.23	2.0000
$5p_{1/2}$	-50.29	2.0	-84.06	2.0000	-103.16	2.0000
$5p_{3/2}$	-40.40	4.0	-73.90	4.0000	-92.67	4.0000
$5d_{3/2}$	-5.10	4.0	-36.20	1.2052	-53.32	0.5788
$5d_{5/2}$			-35.20	1.2392	-52.15	0.6149
$6s$	-6.35	2.0	-31.99	0.0996	-45.45	0.0242
$6p_{1/2}$			-25.14	0.0034	-37.44	0.0017
$6p_{3/2}$			-23.47	0.0030	-35.25	0.0016
$N_{\rm bound}$		74.0		70.5504		69.2204
q		0.0		3.4496		4.7796

Calculations showed that only valence $5d_{3/2}$ and $5d_{5/2}$ states have large occupation numbers while other excited states involving in calculations, that is, $5f$, $6d$, $6f$, $7d$, $7s$, $7p$, $8s$, and $8p$ have zero occupation numbers. The $6p$ states have very small occupation numbers which decrease when temperature increases. We see that increasing temperature causes binding energies to become lower, especially for outer levels. Consequently, the energy spectrum depends considerably on a plasmas temperature, the changes being different for inner and outer levels.

We see that results are different for a free neutral atom and for calculations with regard to a temperature. It should be noted that it was just calculations for a free neutral W atom which were adopted in paper by [J. Abdallah *et al.* (2011)] as initial data. In this paper, the average ionization stage $< q >= 2.07$ was obtained in the collisional radiative model of plasmas for tungsten ion at the electron density $N_e = 10^{14}\mathrm{cm}^{-3}$ and $kT = 2$ eV. The largest contribution were made by transitions $5d^36s^1 \rightarrow 5d^36p^1$ and $5d^4 \rightarrow 5d^36p^1$. It means that the $5d, 6s$, and $6p$ states are of first importance in their calculations as in ours. The ionization stage obtained in our calculations $q = 3.45$. So we believe that our results could be used as initial data in more sophisticated calculations instead data for a free neutral atom. This may change results of these calculations.

In conclusion, we list basic results obtained after the 2-nd CRM in Heidelberg.

- Our unified database was supplemented by the RR and photoionization data for ten tungsten ions W^{14+}-W^{23+}.
- The code PLASMASATOM has been elaborated for evaluation of the energy spectrum and the ion charge in LTE plasmas of various densities and temperatures. Our calculations for the iron, aluminium, and uranium ions in dense plasmas are in a good agreement with previous results obtained by other authors using different models and codes.
- New calculations for the tungsten ion in dense plasmas have given the temperature dependence of the energy spectrum and level occupation numbers in a wide temperature range.
- Calculations have been also performed for the impurity tungsten ion in fusion plasmas at low temperature. Results obtained clearly demonstrate an impact of temperature on the energy spectrum and level occupation numbers.